Title Adaptive Finetuning of 3D CNNs with Interpretation Uncertainty for Seismic Fault Prediction

Review Date of submission: 7th February 2023

Contact Corresponding author: Ahmad Mustafa (amustafa9@gatech.edu)

Adaptive Finetuning of 3D CNNs with Interpretation Uncertainty for Seismic Fault Prediction

Ahmad Mustafa*, Reza Rastegar†, Tim Brown†, Gregory Nunes†, Daniel DeLilla†, and Ghassan AlRegib*

ABSTRACT

3D CNNs can exploit the full extent of spatial information in seismic volumes to predict faults. They require large quantities of training data, but this issue has been mitigated by training such networks with large amounts of synthetic training data to apply afterwards on real datasets. Because of domain shift, pre-trained networks may fail to perform as expected, emphasizing the need to finetune the network with labels obtained on target data of interest. The mismatch in dimensions of network input and interpreter annotations (mostly 2D slices) poses a problem in this respect. In addition, there is a high degree of uncertainty attached to such labels, both on a coarse level as well as on a more fine-grained basis. On an image level, the interpreter may only annotate structures in a small, localized portion of the seismic volume. Furthermore, owing to uncertainty regarding the exact delineation of the endpoints of picked faults, interpreters may only label certain segments on the complete fault line. We propose a method whereby we demonstrate a procedure to finetune the pretrained 3D CNNs with sparse 2D labels on target datasets, resulting in the adaption of their weights to better pick faults in the new domains. Secondly, we devise means to incorporate interpretation uncertainty on labels produced for finetuning to generate better, more reliable fault estimations. We validate our findings on various real datasets and demonstrate improved network performance over the pretrained CNN alone. Additionally, we show that incorporating label uncertainty while finetuning leads to better interpretation performance compared to uncertainty-agnostic finetuning.

*Center for Energy and Geo Processing (CeGP), Omni Lab for Intelligent Visual Engineering and Science (OLIVES), School of Electrical and Computer Engineering, Georgia Institute of Technology, Atlanta, GA. † Occidental Petroleum, Greenway Plaza, Houston, TX.

INTRODUCTION

Geological faults are structures characterized by planar fractures or discontinuities in subsurface rock volumes. The movement of impermeable sedimentary rocks along the fault plane causes the formation of structural traps for hydrocarbons released by source rocks and migrating upward to the reservoir rocks (Sorkhabi and Tsuji, 2005). As such, faults form an essential element of petroleum systems. Processed seismic data acquired over potential drill sites provides a 3D view into the subsurface. Identifying faults on seismic volumes is an important task for seismic interpreters to reduce drilling uncertainty and increase the chances of success of obtaining recoverable hydrocarbons.

Manual interpretation of faults on 3D seismic volumes is a time-consuming, laborious process performed by trained geophysics experts. The recent years have witnessed a tremendous growth in the size and volume of seismic data acquired, rendering manual interpretation impractical in many cases owing to the fast turn-around times required. Deep learning (DL) is a branch of machine learning concerned with automatically learning useful representations from raw data and their corresponding target labels in various everyday tasks of practical interest such as image classification, object detection, and speech recognition (Deng et al., 2013; Erhan et al., 2014; Guo et al., 2017).

Data-driven methods including DL-based models are also being increasingly adopted for interpretation tasks on seismic volumes. (Wang et al., 2018) provide a review of image processing techniques used to automate interpretation of salt domes and faults on seismic volumes. The works by Di et al. (2018) and Guo et al. (2020) describe the use of multi-layer perceptrons (MLPs) and convolutional neural networks (CNNs) to perform fault mapping after training on seismic data with fault labels. Deep learning models trained in a fully supervised manner carry the risk of under-performing when the test data happens to be from a different distribution from the training data or when there is insufficient labeled training data to allow the models to adequately generalize to unseen data.

Recently, there have been a significant number of works in the literature introducing various learning paradigms to relax the assumption of availability of large quantities of labeled training data for machine learning models. Alaudah et al. (2019a) perform weakly supervised learning to identify various structures of interest inside seismic volumes. The works by Alfarraj and AlRegib (2019) and Mustafa et al. (2019) introduce the concepts of sequence models to use in conjunction with the physics-based forward model and limited amounts of labeled data to better estimate subsurface elastic properties from seismic data. Mustafa et al. (2021) use a novel joint learning framework for elastic property estimation tasks under limited labeled data settings. Mustafa and AlRegib (2021) use the neural network's learned manifold to actively identify important training samples for labeling to reduce annotation effort for interpreters.

For structural interpretation, obtaining sufficiently large quantities of labeled training data presents a major bottleneck for any supervised learning-based automation framework. This is owing to multiple factors including the size and complexity of the data, the time and effort required to produce such annotations, and the often-times high level of uncertainty present while assigning particular labels to individual pixels in noisy and complex seismic data. In the work by Wu et al. (2019), the authors put forward a major development in this regard; they demonstrate a framework whereby a large variety of 3D synthetic fault models and their corresponding seismic data are generated and used to train a 3D CNN for the task of fault mapping. Afterwards, the trained network is used to predict faults on real-world target datasets. Their proposed method offers several benefits compared to previous works: firstly, it enables the use of 3D CNNs to extract three-dimensional information in seismic volumes whereas 2D networks, while easier to train, are limited to observe seismic data in 2D patches; secondly, they are able to generate adequate amounts of training data with high-quality labels to allow for sufficient network generalization to unseen test data.

However, the interpretation strategy outlined above falls short in addressing a crucial failure point for deep neural networks: domain shift. Domain shift (Sankaranarayanan et al., 2018) refers to the phenomenon that occurs when neural networks encounter test data sampled from a different distribution than the training data, leading it to underperform. At times, the performance degradation may happen simply due to the test data being processed differently compared to the training data. Specifically in the context of fault interpretation, domain shift may manifest itself in two ways: firstly, synthetic data may not be able to fully model all or even most kinds of real-world fault behavior; secondly, differences in processing styles, acquisition parameters including source wavelet frequency, noise characteristics, subsurface geometry etc., between synthetic and real data may reduce the utility of the pretrained machine learning model. A simple fix for domain-shift might entail acquiring a limited number of labeled data samples in the target domain and retraining the original network with the new data samples, in a process also referred to as finetuning. Appropriately finetuning a pretrained network results in the model retaining beneficial information learned from the original training data while simultaneously adapting to the characteristics of the target data.

Despite the potential for finetuning to bridge domain shift between synthetic and target data distributions, traditional finetuning faces challenges on multiple fronts when applied to the task of fault mapping. On the one hand, 3D networks require target data annotated in 3D chunks to be finetuned, which is infeasible for many reasons as explained above. This is unlike 2D networks that are straightforward to finetune with any number of interpreted 2D image slices from the target seismic volume. On the other hand, there is usually a high degree of uncertainty

involved in fault annotations produced on real datasets. This uncertainty may express itself in the fact that it may be easier to interpret faults in a certain region of the seismic image versus those in other regions. Additionally, there is also uncertainty present on a pixel-wise basis whereby the interpreters may not always find it easy to precisely mark the endpoints of a fault pick. Consequently, a great number of faults may go unlabeled in data samples used to finetune the network. Since conventional network training treats all labels as hard ground-truths, this may lead to inaccuracies in the network output on target data.

In this context, we present a finetuning paradigm for 3D CNNs that overcomes both challenges with conventional finetuning described above. To begin with, our proposed method allows 3D networks pretrained on synthetic fault models to be finetuned with sparsely labeled 2D lines extracted from 3D target seismic datasets. This is made possible using an array of image processing techniques described later in the methodology section. Additionally, our proposed method enables the incorporation of fault label uncertainty in data samples used for finetuning. This is achieved firstly by intelligently sampling training data patches based on fault label proximity resulting in confident data samples majorly contributing to the loss function as opposed to data from unlabeled, uncertain regions in the seismic image(s) annotated by the interpreter. Secondly, loss contributions from pixels in data samples are weighed based on their nearness to the fault labels contained in them to reflect interpretation uncertainty away from the main body of the fault pick(s). The net result of both these strategies is that the network learns exclusively from labeled data with less uncertainty and minimizes contribution from data samples with a higher likelihood of label error. We validate the proposed finetuning methodology via case studies on mutliple real datasets and demonstrate a major improvement of the finetuned network's performance over its pretrained baseline counterpart. Additionally, we also empirically demonstrate the superior performance resulted by incorporating label uncertainty over traditional finetuning that treats training labels as hard ground-truths. To the best of our knowledge, this is the first work of its kind demonstrating finetuning of 3D CNNs with 2D labels in conjunction with modeling label uncertainty for seismic interpretation tasks.

LITERATURE REVIEW

Since the popularization of computational algorithms and resources for interpretation, geophysicists have used seismic attributes to help them identify faults and other structural features of interest on migrated seismic volumes. An attribute is essentially a transformation of seismic data to a different domain that better emphasizes key features to the exclusion of the unimportant components. Examples of such attributes include coherence (Marfurt et al., 1999; Alaudah and AlRegib, 2016, 2017), semblance (Marfurt et al., 1998), gradient magnitude (Aqrawi and Boe, 2011) etc. Seismic attributes that model the human visual system (HVS) to interpret key structures have also been proposed, such as in the works by Shafiq et al. (2016) and Shafiq et al. (2017).

Nevertheless, a limitation with attribute-assisted workflows is that the attribute volumes still need to be manually annotated for structural features. Several works in the literature have attempted to overcome this shortcoming by using various kinds of machine learning models trained on labeled seismic data to then predict structures of interest on test data (Wu et al., 2018; Di et al., 2019b,a). Early attempts in this line of work used training configurations where the data would be presented to the model in patches to predict the label on the center pixel of the patch, such as in Wu et al. (2018). Later works employed state-of-the-art CNN-based models to predict class outputs simultaneously on all pixels in a given patch, such as in the work by Alaudah et al. (2019b). To incorporate information from all directions in a 3D seismic volume, Wu et al. (2019) popularized the use of 3D CNN architectures to generate more accurate structure mappings than was possible with only 2D patch-based machine learning models used by earlier works.

The problem of uncertain interpretations in geophysics is well known. In the work by Bond et al. (2007), the authors demonstrate multiple interpretations by various geophysicists on the same dataset, underscoring the need to quantify such uncertainty to improve hydrocarbon predictability. Zhou et al. (2022) empirically illustrate the effects on model performance and generalizability of conflicting, uncertain training labels in the context of image classification. In the domain of seismic interpretation, Alaudah et al. (2019a) propose a weakly-supervised training scheme to identify key structures in seismic volumes based off hand-selected reference exemplars instead of explicit, pixel-wise labels. Other works such as that by Benkert et al. (2021) propose using model forgetting event-based statistics as a potential means to quantify model uncertainty with regards to the training data and incorporate additional training data accordingly.

METHODOLOGY

Network Architecture

The network architecture follows a typical encoder-decoder style configuration based on the popular image segmentation model 'UNet' (Ronneberger et al., 2015). The encoder branch of the architecture serves to progressively downsample input seismic features and extract increasingly abstract representations utilizing three-dimensional convolutional layers. On the other hand, the decoder branch takes the product of the encoder branch as input and sequentially increases its feature resolution through three-dimensional transposed convolutional layers. Skip connections from various stages in the encoder to the corresponding outputs in the decoder help to transmit in-

formation in input features otherwise lost in subsequent downsampling operations in the encoding branch. In addition to the aforementioned global skip connections, the architecture also implements local skip connections at the output of each stage in the encoder and decoder, respectively. The proliferation of skip connections combined with batch normalization and dropout layers throughout the model architecture helps to make network training more robust. The network takes as input small-sized 3D chunks of the seismic volume having dimensions $h \times w \times d$, where h refers to the height, and w and d to the width and depth of the 3D seismic block, respectively. The network's output is a fault probability volume of the same size as the corresponding seismic input. The amplitude of each voxel in the output fault volume represents its probability of belonging to a fault. Tables 1 and 2 describe the layout of the 3D convolutional layers in the encoder and decoder branches of the network, respectively.

In Channels	Out Channels	Kernel Size	Stride
3	16	3	1
16	16	3	1
16	32	2	2
32	32	3	1
32	32	3	1
32	64	2	2
64	64	3	1
64	64	3	1
64	128	2	2
128	128	3	1
128	128	3	1

Table 1: Table describes the layout of convolutional layers in the encoder branch. Rows in gray specify the convolutional layers serving to downsample input activations using a kernel size and stride of 2.

In Channels	Out Channels	Kernel Size	Stride
128	128	2	2
192	64	1	1
192	64	3	1
64	64	3	1
64	64	2	2
96	32	1	1
96	32	3	1
32	32	3	1
32	32	2	2
48	16	1	1
48	16	3	1
16	16	3	1
16	1	1	1

Table 2: Table describes the layout of convolutional layers in the decoder branch. Rows in gray specify the transposed convolutional layers serving to upsample input activations using a kernel size and stride of 2. The output of each upsampling layer is concatenated channel-wise to encoder outputs in the corresponding layer before processed further.

Pretraining and Finetuning Regimen

Using the method described in Wu et al. (2019), large quantities of synthetic seismic data with associated fault labels are generated to train the 3D CNN model described earlier. The seismic data are modeled to contain faults of various orientations, azimuths, and multiplicities to expose the network to a wide variety of fault information during the pretraining stage. Each training sample consists of a 3D seismic data-fault label pair. As mentioned earlier, the seismic data sample and the fault label volume have the dimensions $h \times w \times d$. Each fault label is a binary volume of 0s and 1s, indicating no-fault and fault voxels, respectively. Using mini-batch gradient descent and backpropagation, the network is trained for many epochs to minimize the binary cross entropy (BCE) loss between predicted and ground truth target fault labels on the training dataset.

Since actual data exhibit various fault and noise behavior not always captured by synthetic fault models, it is imperative to finetune the pre-trained network on labels obtained from an interpreter on a real dataset of interest. The caveat with finetuning a 3D CNN model with real-world annotated data is that the latter often occurs as sparse 2D seismic sections within the complete seismic volume. In contrast, the pre-trained model is set up to take in, process, and output seismic data in 3D blocks. In addition, properly accounting for this dimensionality mismatch problem would require the annotators to label at least w successive seismic sections in the target survey of interest, which could very well prove to be impractical in terms of the effort required. To mitigate this shortcoming, a masking strategy is employed whereby the network processes the seismic volume as usual to produce corresponding fault predictions. A pseudo-target fault volume is then created consisting of all zeros except for the voxels interpreted as faults by the interpreter(s), which carry the label 1. The output fault predictions and the target volume are then compared to each other via BCE loss to produce a 3D loss tensor of the exact dimensions as the network fault output. Finally, the 3D tensor is masked in all places except for the 2D line containing ground-truth interpretations, which is then summed and back-propagated to finetune the network. The masking process is summarized in Figure 1.

Label Uncertainty-aware Sampling

While annotating seismic sections for structures like faults, it is commonplace for seismic interpreters to only annotate faults in a particular target region of the seismic volume, termed the area of interest (ROI). This label inaccuracy can also result from the interpreters either missing subtle faults or mislabeling them as non-faults owing to

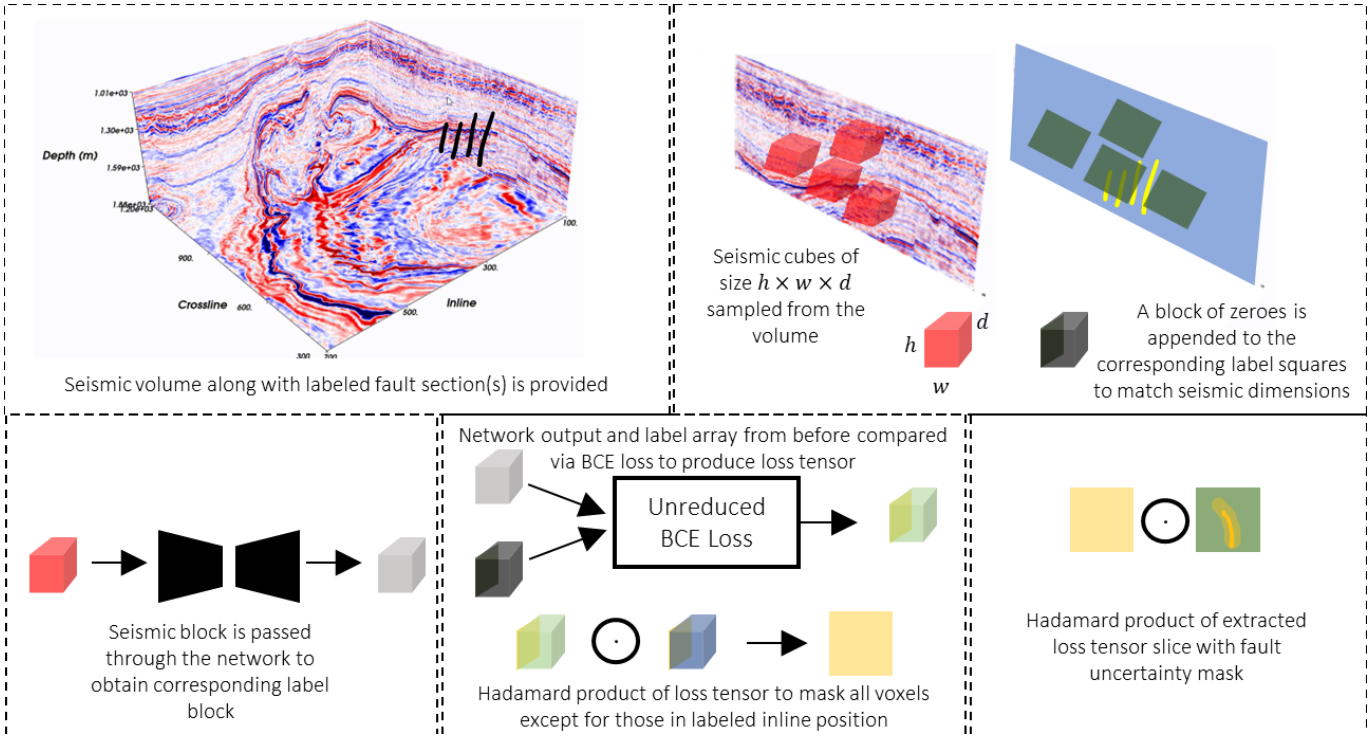

Figure 1: Figure describes the process to finetune 3D CNN-based fault prediction network with sparse 2D labels on select sections in a given seismic volume.

uncertainty in the data. The labels produced as a result of such an annotation process contain ones on all voxels interpreted as faults and zeroes everywhere else, including the fault locations outside the ROI. A typical data-splitting strategy employed by interpretation frameworks evenly divides labeled seismic sections into overlapping blocks across their length and height. There are two significant drawbacks associated with such splitting schemes: firstly, given the sparsity of fault labels, they expose the network to a lot more data points with no faults versus those containing some amount of fault pixels, leading to a class imbalance problem; secondly, inaccurately annotated fault pixels are treated as non-faults. Training the network with such labels would result in the machine learning model incorrectly learning to predict faults outside the ROI as non-fault locations, which may ultimately harm the network's generalization performance on unseen test data samples.

To address this shortcoming with fault labels on seismic sections and their negative ramifications during the training phase, we use a modified data sampling strategy whereby seismic data and their corresponding labels are sampled in 3D chunks centered on the 2D sections labeled by the interpreters *non-deterministically in the locality of annotated fault pixels*. The locations of the fault pixels, as obtained from the annotations, are used as the center points for the cubic data samples (measuring $h \times w \times d$ samples). This allows us to extract training data with less label uncertainty compared to regions of the seismic volume on or outside the ROI's periphery. A drawback of this sampling strategy is that it would only expose the network to seismic data in the immediate neighborhood of the labeled fault pixels. To mitigate this problem, we impose a Poisson distribution whereby the actual sampling locations are a random function of 2D Poisson distributions with the labeled fault pixels as their means.

To illustrate the sampling process, let $\mathcal{I}$ be the set of labeled fault positions for a target seismic volume, where $\mathcal{I} = \{(a^{(i)}, b^{(i)}, c^{(i)})\}_{i=1}^{N}$. $a^{(i)}$, $b^{(i)}$, and $c^{(i)}$ refer to the height, crossline, and inline position of the i-th fault pixel, respectively. N refers to the total number of labeled fault pixels of the volume. Since N may be extremely large even for moderately sized seismic volumes, we select a smaller subset of pixel indices termed $\mathcal{I}'$ of size N', where $\mathcal{I}' \subseteq \mathcal{I}$ and $N' << N$. To avoid having redundant training samples within the proximity of a few pixels, we first randomly permute the ordering of elements in $\mathcal{I}$ to then select the first N' index locations. During the training stage, each index tuple in $\mathcal{I}'$ is used to extract cubic samples from both the seismic and the corresponding label data, as described in the previous section. To prevent the network over-training on the same set of predetermined N' locations, we inject randomness into the sampling criteria by drawing index locations from Poisson distributions centered on the pixel indices instead of using the latter. In each iteration, an index tuple is sampled from $\mathcal{I}'$ as

$$(a^{(i)}, b^{(i)}, c^{(i)}) \sim \mathcal{I}'. \tag{1}$$

The actual sampling indices are then obtained as random samples from a multidimensional poisson distribution

as

$$(a_s^{(i)}, c_s^{(i)}) \sim \text{poisson}(a^{(i)}), \text{poisson}(c^{(i)}). \quad (2)$$

Notice that we only perturb the height and inline indices and let the crossline position stay constant. This is because the latter specifies the position of the labeled 2D line in the seismic volume and it is used to perform tensor masking as described in the previous section. Using these indices, the i-th cubic data sample $x^{(i)}$ is obtained from the seismic volume tensor S as

$$\begin{aligned} x^{(i)} = S[a_s^{(i)} - \frac{h}{2} : a_s^{(i)} + \frac{h}{2}, \\ b^{(i)} : b^{(i)} + w, \\ c_s^{(i)} - \frac{d}{2} : c_s^{(i)} + \frac{d}{2}], \end{aligned} \quad (3)$$

where h refers to the height, and w and d to the width and depth of the 3D seismic block, respectively. Sampling training labels in this manner has two benefits: it firstly serves to circumvent the class imbalance problem resulted from an outnumbering of non-fault locations over those with fault; secondly, it reduces the likelihood of misannotated regions being used to train the network by concentrating most samples in the proximity of labeled fault positions. Additionally, injecting randomness into sampling locations increases the effective size of the training dataset and ensures the network learns the full manifestation of fault characteristics in the labeled seismic section. Figure 2(a) compares a typical data sampling strategy deployed in deep learning workflows to the proposed sampling strategy in Figure 2(b). As mentioned earlier, the conventional sampling method results in class imbalance in addition to generating a lot of samples with incorrect/uncertain labels. In contrast, the proposed method focuses on extracting data in the neighborhood of the annotated fault, thus mitigating both problems with the conventional strategy.

Fault Distance-based Weighting of the Loss Tensor

Uncertainty regarding fault positions on a seismic image may happen on an image level, where certain regions of interest are easier to interpret compared to other regions. The previous section described one possible means to address this problem. However, there may also be another kind of uncertainty present: that on a pixel level. Within the same region of interest, pixels closer to the fault plane may have less label uncertainty attached to them compared to pixels further away. A practical example of this is how when it is not always possible to specify with one hundred percent certainty the endpoints of a delineated fault. To incorporate this uncertainty into the training regime, we use a weighting mask that emphasizes the loss contribution from each pixel for a given training sample based off its nearness to the fault plane. Pixels closer to the annotated fault contribute more to the loss function and vice versa.

In the first step of this process, we obtain the 3D loss tensor resulting from the pixel-wise binary cross entropy between the predicted and ground-truth fault cube. Since the actual fault annotation by interpreters is only present on a single 2D section of this tensor, we extract this one section from the tensor (measuring $h \times d$ samples) and mask out everything else so that un-annotated pixels do not affect the loss function. Let this 2D loss tensor be denoted by the discrete function $l[m, n]$, where $0 \leq m \leq h$ and $0 \leq n \leq d$. Let the set $\mathcal{G}$ stand for all such pixel locations (m, n) in the tensor. A mathematical function, F is formulated that maps each tuple $(m, n) \in \mathcal{G}$ to the straight-line distance value d ($d \in \mathbb{R}$) between the said pixel location and the nearest fault pixel in the given data cube. This is described by the mapping $F : \mathcal{G} \to \mathbb{R}$, and laid out in more detail as the optimization problem

$$F[m, n] = \min_{(m', n') \in x} (m - m')^2 + (n - n')^2, \quad (4)$$

where m' and n' refer to the height and width indices, respectively, for all annotated fault pixel positions in the given data cube x. The weighting function, $w[m, n]$ is then obtained as

$$w[m, n] = \alpha e^{-\gamma F[m,n]}, \quad (5)$$

where the negative exponential of F is taken to convert low distances to high weights and vice versa. α is a hyperparameter specifying the positive emphasis applied to pixel locations close to annotated fault pixels. γ is another hyper-parameter controlling the steepness of the drop from large positive weight values. Finally, the loss value is obtained as

$$\text{loss} = \sum_{m,n} l[m, n] \circ w[m, n], \quad (6)$$

where '$\circ$' refers to the Hadamard product between the original loss tensor and the weight mask. 2D slices from a seismic cube sample, its corresponding data label, and the generated pixel weights are shown in Figure 2(c).

EXPERIMENTS AND RESULTS

Case Study I: F3 Block Migrated Seismic Volume

We validated the label uncertainty-aware finetuning strategy on two different datasets. The first dataset was obtained from the Netherlands offshore F3 block and consists of a migrated seismic volume that was interpreted by the authors in Alaudah et al. (2019b) for six different lithostratigraphic units. The seismic volume used for the study consists of 401 inlines, 701 crosslines, and 255 depth samples. For finetuning our network pretrained on synthetic fault data, we manually annotated some of the major faults in the deeper section of the first inline. A 3D view of the seismic volume along with the first inline image and its corresponding fault annotations are shown in Figure 3.

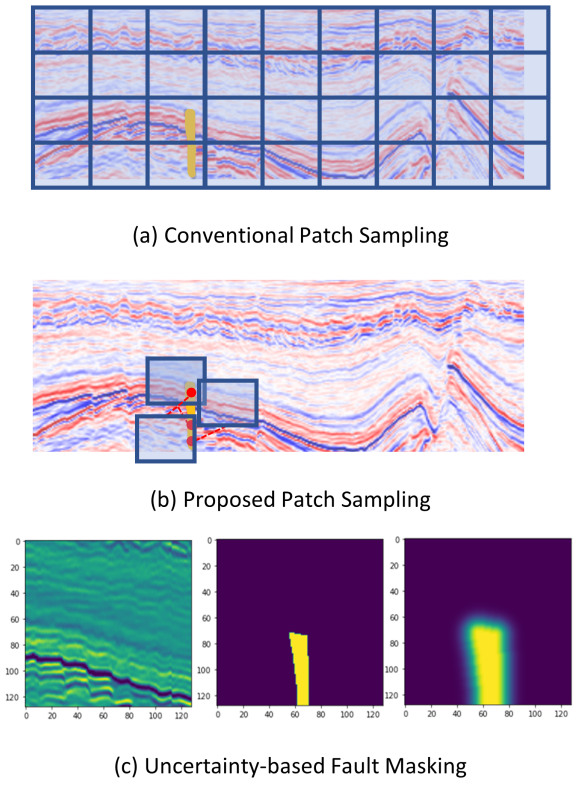

Figure 2: Conventional fault cube extraction strategy (a) compared and contrasted with proposed cube extraction method (b). Fault label is shown in yellow superimposed on the seismic image. Blue squares represent sampling locations. (c) shows pixel weights for the loss tensor corresponding to one seismic data sample and its corresponding label tensor. Note that the method itself samples 3D tensors, but for ease of understanding, we show the relevant 2D slices.

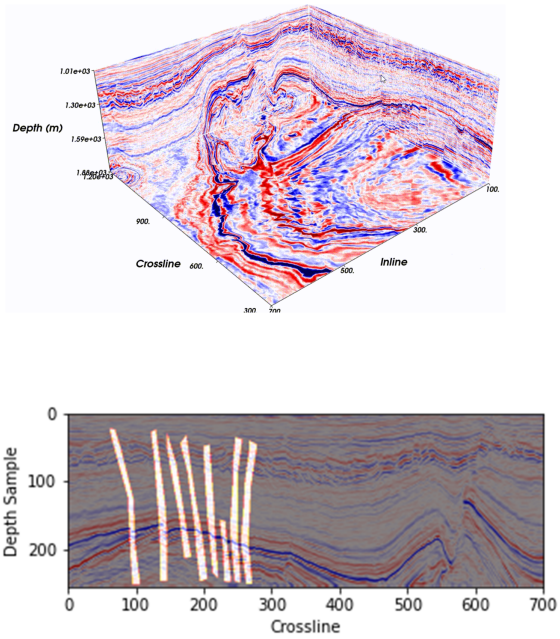

Figure 3: Figure shows the seismic volume from the F3 block (above) and fault annotations on the first inline (below).

The pretrained network is finetuned on the first inline in the manner described earlier for five epochs using a learning rate of $1e-4$ and the adaptive moment estimation (ADAM) optimizer (Mehta et al., 2019). The script is written using Python and the popular deep learning package PyTorch (Pytorch, 2018). We specify N' to be 100, α to be 10, and γ to be 0.01. The finetuned model is afterwards used to perform inference on the original seismic volume whereby the volume is split evenly into 3D blocks, passed through the network, and the results stitched together to produce the final model predictions. The window size for block dimensions h, w, and d are set to 128 for both training and inference. Figure 4 shows fault outputs on three randomly picked inlines in the F3 seismic volume before and after finetuning (left and right columns, respectively).

Case Study II: Thebe Gas Field Seismic Volume

The second case study is performed on a seismic volume from the Thebe gas field on the north-western shelf of Australia. The survey site lies on the Exmouth plateau of Carnarvon basin. The migrated seismic images were annotated for the presence of faults in the deeper section of the volume by a team of experts, as described in the work by An et al. (2021). The final, processed seismic volume consists of 1807 crosslines, 3174 inlines, and 1537 samples in depth. As before, a single inline section from the volume and its associated fault labels are used to finetune the network pretrained on synthetic data. The hyperparameter settings are kept to similar levels as before. In addition, we also manually downsample the seismic volume and its labels by a factor of three so as not to exceed our limited CPU and GPU memory budget during the training and inference phases. After performing inference with the finetuned model on the original seismic volume, the model outputs before and after finetuning are plotted along with the ground-truths in Figure 5.

Proposed Approach Versus Regular Finetuning Under Severe Label Uncertainty

To demonstrate the advantages of the proposed finetuning method over regular finetuning, we simulated a scenario with the F3 block seismic volume where the annotations for the first inline section contained a large amount of label uncertainty. This is shown in the upper-most plot in Figure 6. Compared to the annotations in Figure 3, it is obvious only a small fraction of the previously labeled faults were annotated. We then proceeded to finetune our pretrained network using both the uncertainty-aware strategy outlined before as well as regular finetuning that does not account for label uncertainty. The network outputs for both approaches on the first inline during inference can be seen in the middle and bottom plots in Figure 6. The proposed method (middle) can be observed to outperform uncertainty-agnostic finetuning even in the absence of a significant number of fault labels. This is because the latter treats pixel labels as the absolute ground truth that results in many fault pixels being inaccurately treated as non-faults. In addition, it employs a uniform cube extraction strategy that produces a large degree of class imbalance in the data, with the number of cubes with little to no fault pixels far outnumbering those with a significant number of fault pixels. The former on the other hand focuses its attention in the proximity of fault pixels and minimizes loss contribution of pixels further away. This increases the chances of the machine learning model not only learning the labeled fault behavior well, but also generalizing better to pixels inaccurately labeled as non-faults.

DISCUSSION

The preceding analysis demonstrated the superior performance of the proposed method over the network trained only on synthetic data in two ways: firstly, it can be observed that finetuning produces more confident and more continuous fault picks on test data compared to the pretrained network. This can be very notably observed on inline 133 (top row) in Figure 4 where the finetuned network can be seen to capture the full extent of faults in the lower left section of the image better compared to its baseline counterpart that is only able to identify isolated segments of the actual fault lines. This behavior is also depicted in fault predictions generated on the Thebe Gas Basin data as shown on the various inline sections in Figure 5. Secondly, the finetuned network is able to pick faults not annotated at all in the labeled data provided for finetuning. This is demonstrated very noticeably in the shallow sections of the various inline images in Figure 4. In contrast, the pretrained network is not able to identify such faults at all. This is also seen in the upper halves of inline images selected for model validation on the Thebe Basin in Figure 5.

These results are explained by our earlier discussion on domain shifted test data causing the pretrained network to underperform. Finetuning helps to bridge the gap between training and test data distributions and adapts the network's weights towards identifying the unique way faults manifest themselves in the target data. This helps the network to both make more reliable estimations on annotated faults as well as pick up unannotated faults in the target domain. The pretrained network is able to map faults in the target data in so far as the fault features therein exhibit similarity to those in the training data. However, in cases where the training data does not fully model real-world fault behavior, it produces relatively suboptimal predictions.

We would also like point out future directions and rooms for improvement to the proposed methodology. It should be emphasized that the method to incorporate label uncertainty into the finetuning process is independent of the choice of the network configuration; the label uncertainty

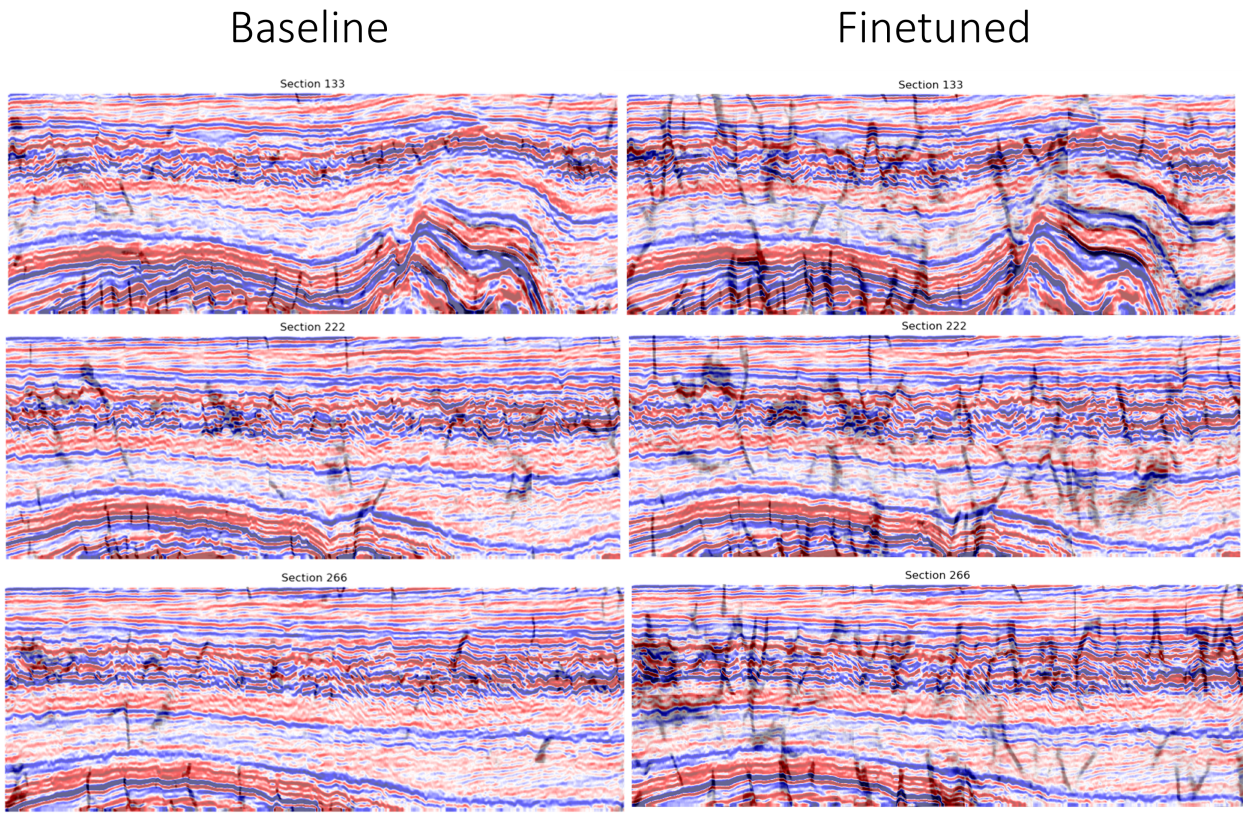

Figure 4: Figure 4 shows fault outputs in black superimposed on three randomly picked inlines (133, 222, and 266, respectively) in the F3 seismic volume before and after finetuning (left and right columns, respectively).

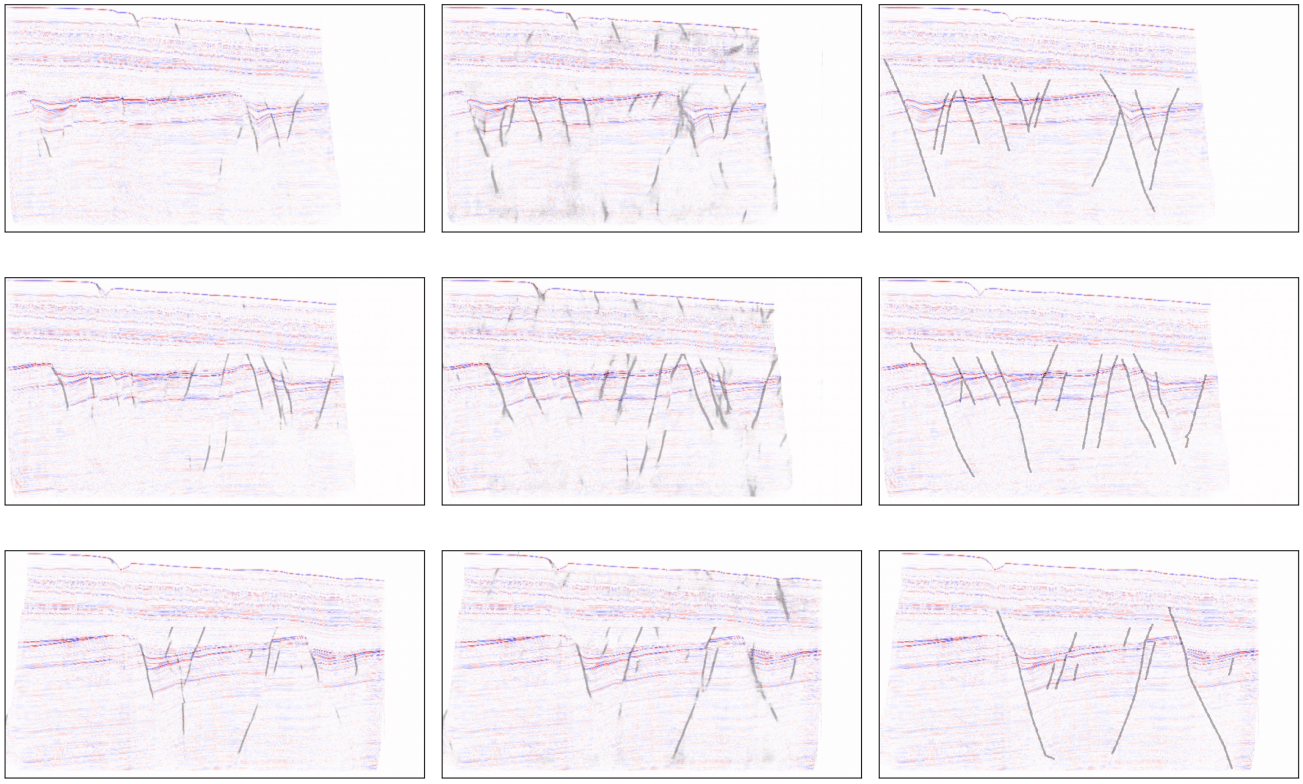

Figure 5: Figure shows fault outputs in black superimposed on three randomly picked inlines (50, 150, and 350, respectively) in the Thebe gas field seismic volume before and after finetuning (left and middle columns, respectively). The ground-truth annotations by interpreters are depicted in the right column.

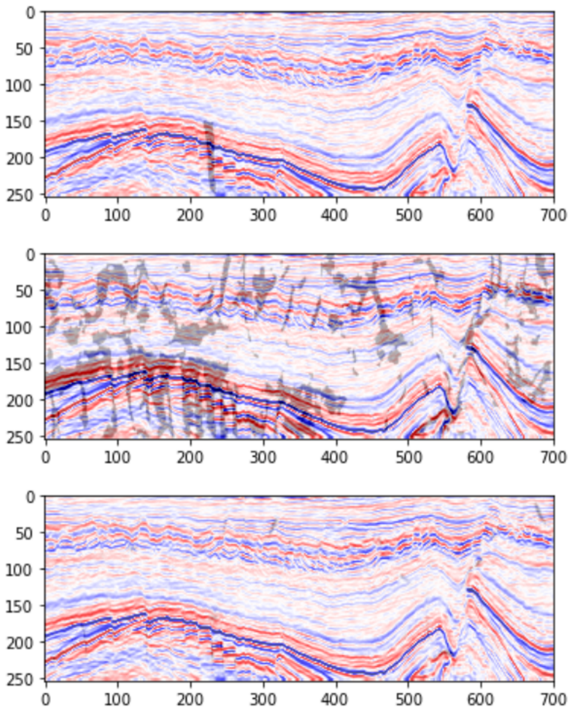

Figure 6: Fault annotations containing a large degree of uncetainty (top) are used to finetune the pretrained network using both the proposed and regular finetuning strategies. The proposed, uncertainty-aware approach (middle) can be seen to outperfrom uncertainty-agnostic finetuning (below) at picking both the labeled and unlabeled faults.

could as easily have been adapted to an interpretation setup employing a different 3D CNN or even 2D CNNs. Given that uncertainty in the labels is almost a given for any interpretation project, the proposed method provides a convenient means to incorporate this error into machine learning-based interpretive frameworks. As such, ablation studies of the proposed method used in conjunction with different architectures and training configurations would considerably assist in the realization of robust human-in-the-loop seismic interpretation systems.

Additionally, it should be pointed out that at present, the proposed technique only accounts for uncertainty in the fault class, and not the non-fault pixels. Incorporating label confidence for non-fault regions into the finetuning method would allow the machine learning model to generalize well to not only fault instances, but also to cases where it should not predict faults, as in the proximity of the salt domes in Figure 4.

Moreover, the proposed approach adopts only one kind of label error model that assumes high confidence close to fault picks produced by interpreters and low confidence the further one moves away from such regions. This is based on typical human visual attention models focusing more attention onto specific regions of interest and less attention to places further away. However, there is considerable room to explore the use of other uncertainty models including ones based on image quality characteristics in seismic images. Such uncertainty models would impose high label confidence in image regions of high quality and likewise assume low label confidence for regions containing noise and other degradation-related phenomena.

CONCLUSION

The paper discussed limitations to existing fault interpretation strategies that deploy 3D CNNs trained on large numbers of synthetic fault data samples in terms of such models usually performing poorly on real target data not accurately modeled by synthetic data. Finetuning such networks with sparsely labeled 2D lines from target datasets of interest is one potential solution to the domain shift problem. However, training 3D networks with sparse 2D labels poses an intractable problem owing to dimensionality mismatch between the network and input data configurations. Moreover, conventional finetuning does not take label uncertainty on target data samples into account. We proposed a training paradigm that firstly allows for training 3D networks with any number of sparse 2D slices taken from a seismic volume, overcoming the data dimensionality mismatch problem. Secondly, we put presented means to incorporate label confidence into the finetuning process so that the network maximizes learning from high-confidence labeled samples and minimizes contribution from low-confidence, error-prone data samples. We validated the proposed technique on various real case studies and demonstrated improved network performance with finetuning over the baseline pretrained counterpart. It is hoped that this work will set the foundation

for future research into modeling uncertainty and label confidence for machine learning-based structural interpretation tasks.

REFERENCES

Alaudah, Y., M. Alfarraj, and G. AlRegib, 2019a, Structure label prediction using similarity-based retrieval and weakly supervised label mappingstructure label prediction: Geophysics, **84**, no. 1, V67–V79.

Alaudah, Y., and G. AlRegib, 2016, A generalized tensor-based coherence attribute: 78th EAGE Conference and Exhibition 2016, European Association of Geoscientists & Engineers, 1–5.

———, 2017, A directional coherence attribute for seismic interpretation: Presented at the 2017 SEG International Exposition and Annual Meeting, OnePetro.

Alaudah, Y., P. Michałowicz, M. Alfarraj, and G. AlRegib, 2019b, A machine-learning benchmark for facies classification: Interpretation, **7**, no. 3, SE175–SE187.

Alfarraj, M., and G. AlRegib, 2019, Semi-supervised learning for acoustic impedance inversion, *in* SEG Technical Program Expanded Abstracts 2019: Society of Exploration Geophysicists, 2298–2302.

An, Y., J. Guo, Q. Ye, C. Childs, J. Walsh, and R. Dong, 2021, A gigabyte interpreted seismic dataset for automatic fault recognition: Data in Brief, **37**, 107219.

Aqrawi, A. A., and T. H. Boe, 2011, Improved fault segmentation using a dip guided and modified 3d sobel filter, *in* SEG Technical Program Expanded Abstracts 2011: Society of Exploration Geophysicists, 999–1003.

Benkert, R., O. J. Aribido, and G. AlRegib, 2021, Explaining deep models through forgettable learning dynamics: 2021 IEEE International Conference on Image Processing (ICIP), IEEE, 3692–3696.

Bond, C. E., A. D. Gibbs, Z. K. Shipton, S. Jones, et al., 2007, What do you think this is¿'conceptual uncertainty"in geoscience interpretation: GSA today, **17**, no. 11, 4.

Deng, L., G. Hinton, and B. Kingsbury, 2013, New types of deep neural network learning for speech recognition and related applications: An overview: 2013 IEEE international conference on acoustics, speech and signal processing, IEEE, 8599–8603.

Di, H., D. Gao, and G. AlRegib, 2019a, Developing a seismic texture analysis neural network for machine-aided seismic pattern recognition and classification: Geophysical Journal International, **218**, no. 2, 1262–1275.

Di, H., M. Shafiq, and G. AlRegib, 2018, Patch-level mlp classification for improved fault detection, *in* SEG Technical Program Expanded Abstracts 2018: Society of Exploration Geophysicists, 2211–2215.

Di, H., M. A. Shafiq, Z. Wang, and G. AlRegib, 2019b, Improving seismic fault detection by super-attribute-based classification: Interpretation, **7**, no. 3, SE251–SE267.

Erhan, D., C. Szegedy, A. Toshev, and D. Anguelov, 2014, Scalable object detection using deep neural networks: Proceedings of the IEEE conference on computer vision and pattern recognition, 2147–2154.

Guo, T., J. Dong, H. Li, and Y. Gao, 2017, Simple convolutional neural network on image classification: 2017 IEEE 2nd International Conference on Big Data Analysis (ICBDA), IEEE, 721–724.

Guo, Y., S. Peng, W. Du, and D. Li, 2020, Fault and horizon automatic interpretation by cnn: a case study of coalfield: Journal of Geophysics and Engineering, **17**, 1016–1025.

Marfurt, K. J., R. L. Kirlin, S. L. Farmer, and M. S. Bahorich, 1998, 3-d seismic attributes using a semblance-based coherency algorithm: Geophysics, **63**, no. 4, 1150–1165.

Marfurt, K. J., V. Sudhaker, A. Gersztenkorn, K. D. Crawford, and S. E. Nissen, 1999, Coherency calculations in the presence of structural dip: Geophysics, **64**, no. 1, 104–111.

Mehta, S., C. Paunwala, and B. Vaidya, 2019, Cnn based traffic sign classification using adam optimizer: 2019 International Conference on Intelligent Computing and Control Systems (ICCS), IEEE, 1293–1298.

Mustafa, A., M. Alfarraj, and G. AlRegib, 2019, Estimation of acoustic impedance from seismic data using temporal convolutional network, *in* SEG Technical Program Expanded Abstracts 2019: Society of Exploration Geophysicists, 2554–2558.

———, 2021, Joint learning for spatial context-based seismic inversion of multiple data sets for improved generalizability and robustness: Geophysics, **86**, no. 4, O37–O48.

Mustafa, A., and G. AlRegib, 2021, Man-recon: manifold learning for reconstruction with deep autoencoder for smart seismic interpretation: 2021 IEEE International Conference on Image Processing (ICIP), IEEE, 2953–2957.

Pytorch, A. D. I., 2018, Pytorch.

Ronneberger, O., P. Fischer, and T. Brox, 2015, U-net: Convolutional networks for biomedical image segmentation: International Conference on Medical image computing and computer-assisted intervention, Springer, 234–241.

Sankaranarayanan, S., Y. Balaji, A. Jain, S. N. Lim, and R. Chellappa, 2018, Learning from synthetic data: Addressing domain shift for semantic segmentation: Proceedings of the IEEE conference on computer vision and pattern recognition, 3752–3761.

Shafiq, M. A., T. Alshawi, Z. Long, and G. AlRegib, 2016, Salsi: A new seismic attribute for salt dome detection: 2016 IEEE International Conference on Acoustics, Speech and Signal Processing (ICASSP), IEEE, 1876–1880.

Shafiq, M. A., Z. Wang, G. AlRegib, A. Amin, and M. Deriche, 2017, A texture-based interpretation workflow with application to delineating salt domes: Interpretation, **5**, no. 3, SJ1–SJ19.

Sorkhabi, R., and Y. Tsuji, 2005, The place of faults in

petroleum traps.

Wang, Z., H. Di, M. A. Shafiq, Y. Alaudah, and G. AlRegib, 2018, Successful leveraging of image processing and machine learning in seismic structural interpretation: A review: The Leading Edge, **37**, no. 6, 451–461.

Wu, X., L. Liang, Y. Shi, and S. Fomel, 2019, Faultseg3d: Using synthetic data sets to train an end-to-end convolutional neural network for 3d seismic fault segmentation: Geophysics, **84**, no. 3, IM35–IM45.

Wu, X., Y. Shi, S. Fomel, and L. Liang, 2018, Convolutional neural networks for fault interpretation in seismic images: Presented at the 2018 SEG International Exposition and Annual Meeting, OnePetro.

Zhou, C., M. Prabhushankar, and G. AlRegib, 2022, On the ramifications of human label uncertainty: arXiv preprint arXiv:2211.05871.